– Supporting Material –

Effect of the N-Terminal Helix and Nucleotide Loading on the Membrane and Effector Binding of Arl2/3

Shobhna Kapoor,[1,2,⊥] Eyad K. Fansa,[3,⊥] Simone Möbitz,[1] Shehab A. Ismail,[3,4] Roland Winter,[1] Alfred Wittinghofer,[3,*] and Katrin Weise[1,*]

[1] Physical Chemistry I – Biophysical Chemistry, TU Dortmund University, Otto-Hahn-Strasse 6, 44227 Dortmund, Germany

[2] Department of Chemical Biology, Max Planck Institute of Molecular Physiology, Otto-Hahn-Strasse 11, 44227 Dortmund, Germany

[3] Structural Biology Group, Max Planck Institute of Molecular Physiology, Otto-Hahn-Strasse 11, 44227 Dortmund, Germany

[4] Structural Biology of Cilia, CR-UK Beatson Institute, Garscube Estate Switchback Road, Glasgow G61 1BD, United Kingdom

*Correspondence:
katrin.weise@tu-dortmund.de or alfred.wittinghofer@mpi-dortmund.mpg.de

Author Contribution:
[⊥] Shobhna Kapoor and Eyad K. Fansa contributed equally to this work.

MATERIALS AND METHODS

Surface plasmon resonance (SPR)

SPR experiments were carried out with a Biacore 3000 system (Biacore, Uppsala, Sweden; now GE Healthcare). For the protein-membrane interaction studies, the pioneer L1 sensor chip (GE Healthcare, Munich, Germany) was used that is composed of a thin lipophilic modified dextran matrix on a gold surface, upon which lipid bilayers can be immobilized through the capture of liposomes by the lipophilic compounds (1,2). The chip has been shown to be suitable for the generation of model membrane systems that provide a flexible lipid bilayer surface that closely resembles the surface of a cellular membrane (3,4). All measurements were carried out at a temperature of 25°C, with the samples cooled at 10°C in the autosampler before the measurement was started.

Prior to the experiment, the L1 chip was primed 4× with Hepes buffer (10 mM Hepes, 5 mM $MgCl_2$, 150 mM NaCl, pH 7.5). Afterwards, the chip surface underwent a cleaning program by injecting 30 µL 2-propanol / 50 mM NaOH (2:3), 10 µL octyl β-D-glucopyranoside (40 mM), and 30 µL Chaps (20 mM), NaCl (100 mM), and $CaCl_2$ (20 mM) at a flow rate of 5 µL/min. For vesicle immobilization, 15 µL of the extruded lipid vesicle solution (0.5 mM) were injected twice at a flow rate of 2 µL/min, which was followed by a stabilization phase by injecting 50 µL of Hepes buffer at a flow rate of 100 µL/min and three further injections of 10 µL 25 mM NaOH at a flow rate of 5 µL/min. Finally, the lipid surface was stabilized by injecting 40 µL Hepes buffer at a flow rate of 20 µL/min. After baseline stabilization, 40 µL of the protein containing solution (c_{Arl} = 2 µM, $c_{UNC119a}$ = 3 µM) were injected at a flow rate of 20 µL/min and the dissociation was followed for 30 min. For the membrane interaction studies with the UNC119a-complexed Arl, both proteins were mixed prior to injection into the SPR flow cell to yield a final concentration of 2 µM Arl and 3 µM UNC119a. After following the dissociation for 30 min, the chip surface was regenerated using the cleaning program. The degree of chip surface coverage with lipids was determined by means of 0.5 µM BSA and was found to be ≥75% for all cases.

To eliminate unspecific binding effects such as the interaction of Hepes buffer with the L1 chip and non-specific binding of the proteins to the pure L1 chip that depend on the determined lipid coverage, these signals were subtracted from the actual sensorgrams of the respective protein solutions. Hence, the ratio of the maximal amplitude of the BSA-membrane and BSA-chip sensorgram yields the amount of the chip surface that is not covered with lipids and is used as a factor for correcting the zeroized (i.e., setting the baseline before injection of the protein solution to zero) protein-chip sensorgram. This corrected sensorgram is then subtracted from the buffer-corrected and zeroized protein-membrane sensorgram to yield the final protein-membrane sensorgram for analysis. All sensorgrams were recorded at a frequency of 10 Hz.

For all measurements performed, the SPR data were analyzed on the basis of a multi-step model owing to the non-simple-exponential association and dissociation curves observed in the sensorgrams for the protein-membrane interaction, reflecting a complex interaction behavior. A two-step reaction model was shown to provide an appropriate curve-fitting algorithm and describes a process with two reaction steps that, in terms of protein-lipid interactions, correspond to:

$$P + L \underset{k_{off,1}}{\overset{k_{on,1}}{\rightleftharpoons}} PL \underset{k_{off,2}}{\overset{k_{on,2}}{\rightleftharpoons}} PL^{*} \quad , \qquad \text{(Scheme 1)}$$

where the soluble protein (P) binds to the immobilized lipids (L) forming a primary binding complex (PL) and a secondary protein-lipid complex (PL*, e.g., a clustered state as shown previously for K-Ras4B by atomic force microscopy (5) and in the present manuscript for Arl2/3). The effect of Arl clustering on the response measured is indirect in altering the equilibrium between the bound and free forms of the protein, allowing a dissociation of PL* only through reversal of the clustering reaction step. To directly obtain values for the association rate constant k_{on}, the whole sensorgram was fitted to the two-step model. The parameters $k_{on,1}$ and $k_{on,2}$ represent the corresponding association rates of the respective reaction steps. Curve fitting was performed by using the Marquardt-Levenberg algorithm and the fitted curves were generated by numerical integration of the differential equations that describe the reaction scheme. This fitting procedure was implemented in the BIAevaluation software 4.1 (Biacore, Uppsala, Sweden). Representative fits of the SPR curves are shown in Fig. S1 (see below). Owing to this complex reaction scheme, the maximum error bars of the fits were sometimes large due to error propagation. Hence, the initial association phase (for $t \rightarrow 0$), which is directly proportional to $k_{on,1}$, was also evaluated by linear regression using Origin 7 (OriginLab Corporation, Northampton, MA, USA), resulting in values for the initial slope of the sensorgram. The model and the corresponding analysis have been described in detail in ref. 1.

Whereas the two-step fit of the whole sensorgram gave reasonable results for the association phase, a larger discrepancy was observed for the fitted dissociation part of the curve. Thus, the dissociation phase was fitted separately to a biexponential model (Eq. 1) using Origin 7, yielding two independent dissociation rate constants $k_{off,1}$ and $k_{off,2}$ as well as their respective contributions A_1 and A_2.

$$R = A_1 \times e^{-k_{off,1}(t-t_0)} + A_2 \times e^{-k_{off,2}(t-t_0)} + \text{offset} \quad (1)$$

t_0 indicates the beginning of the dissociation phase, i.e., the time point when the flow cell switched from protein to buffer solution. The relative amount of quasi-irreversibly bound protein was derived by correlating the offset value of the biexponential fit to the initial amplitude at the starting point ($t = 0$) of the dissociation phase corresponding to the following equation:

$$\text{quasi}-\text{irrevers.} = \frac{\text{offset}}{A_1 + A_2 + \text{offset}} \ . \quad (2)$$

From Eq. 1, an average dissociation rate $\bar{k}_{diss}$ can be calculated:

$$\bar{k}_{diss} = \frac{A_1}{A_1 + A_2} \times k_{off,1} + \frac{A_2}{A_1 + A_2} \times k_{off,2} \ . \quad (3)$$

The error bars in all experiments represent the standard deviation from at least three (up to six) independently conducted experiments, and the corresponding values for all determined kinetic parameters are given in Tables S1–S3.

FIGURES

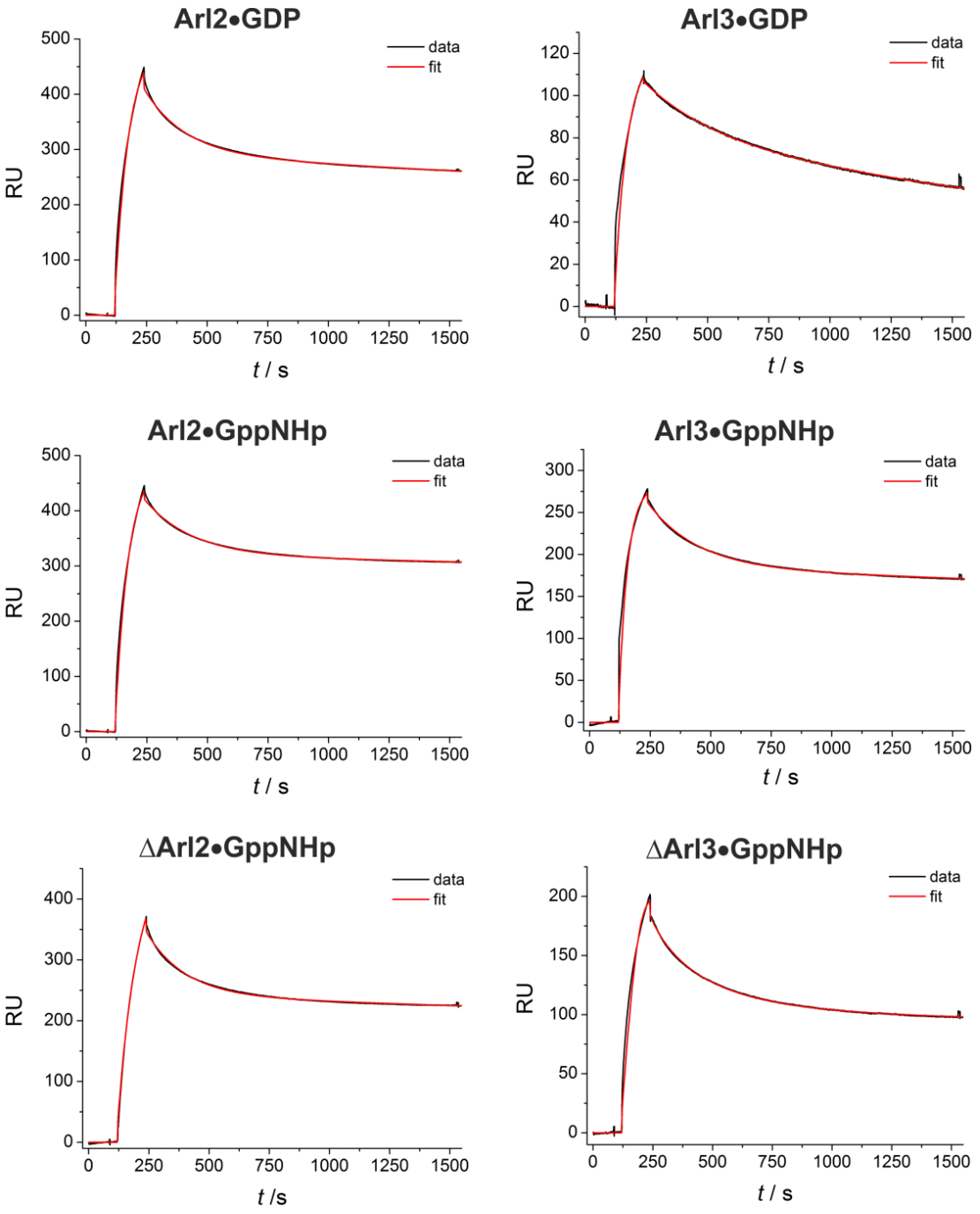

FIGURE S1 Representative fits (red curves) of the SPR sensorgrams (black curves) of the different proteins by use of the Marquardt-Levenberg algorithm, with the fitted curves being generated by numerical integration of the differential equations that describe the two-step reaction scheme (Scheme 1, see above). This fitting procedure was implemented in the BIAevaluation software 4.1 (Biacore, Uppsala, Sweden).

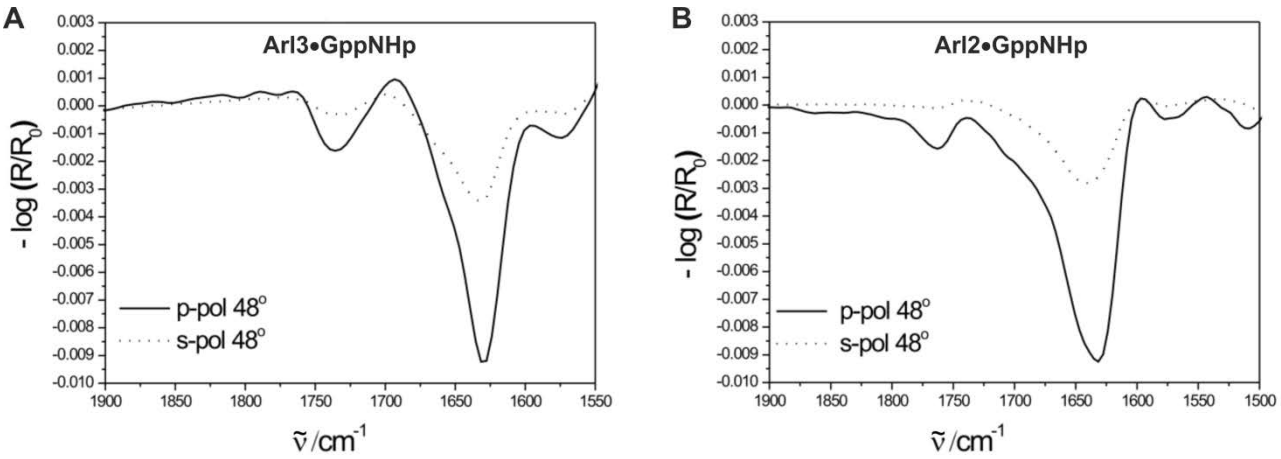

FIGURE S2 Comparison of spectral details between s- and p-polarized light. IRRA spectra for the amide-I′ region of Arl3•GppNHp (A) and Arl2•GppNHp (B) in the presence of anionic raft membranes. All IRRA spectra were recorded with p-polarized or s-polarized light at 48° angle of incidence.

p-polarized IRRAS amide-I′ peaks can be positive or negative depending on the direction of the transition moment of the amide-I′ helices, with respect to the angle of incidence. The main purpose of using p-polarized light for the present study instead of s-polarized light, where all peaks are negative, was mainly to obtain a large signal and better signal-to-noise ratio for membrane-bound proteins. The figure shows the IRRA spectra for membrane-bound Arl2/3 obtained using both p- and s-polarized light at 48° angle of incidence. As can be seen the spectra acquired using p-polarized light have at least 3-fold higher intensity than their s-polarized counterparts, though the wavenumber maximum for the amide-I′ band is the same for both IR radiations, providing the same structural information. This higher intensity obtained by using p-polarized light is explained in detail in theory (6).

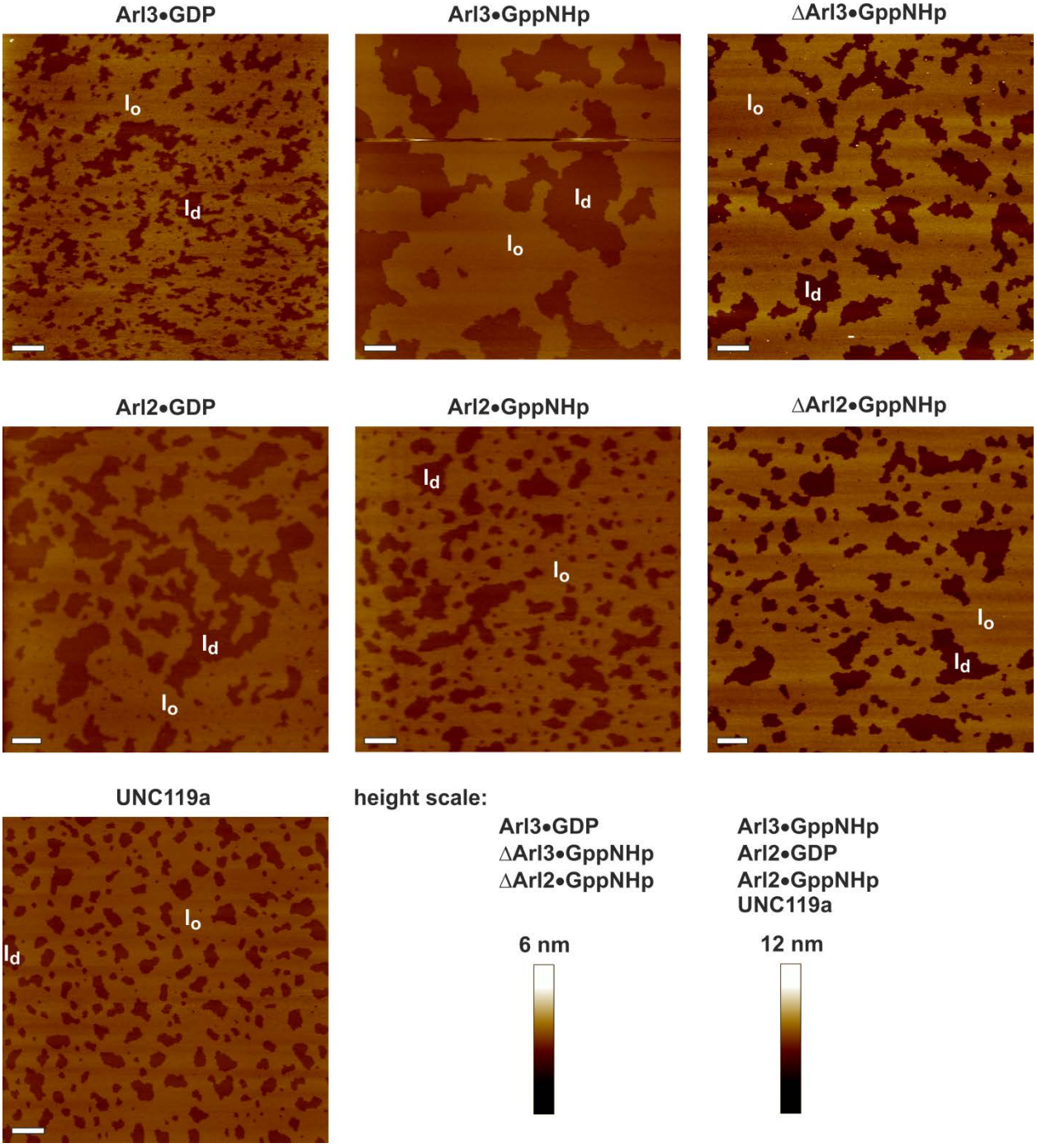

FIGURE S3 AFM images of the anionic model raft membrane consisting of DOPC/DOPG/DPPC/ DPPG/Chol 20:5:45:5:25 (mol %) on mica before addition of the corresponding proteins. All AFM images show a defect-free, continuous lipid bilayer on mica with isolated liquid-disordered (l_d) domains in a liquid-ordered (l_o) membrane matrix at room temperature. The overall height of the vertical color scale corresponds to 6 nm for Arl3•GDP, ΔArl3•GppNHp, and ΔArl2•GppNHp, and 12 nm for Arl3•GppNHp, Arl2•GppNHp, Arl2•GDP, and UNC119a, comparable to the AFM images shown in Fig. 4. The scale bar represents 1 μm for all images.

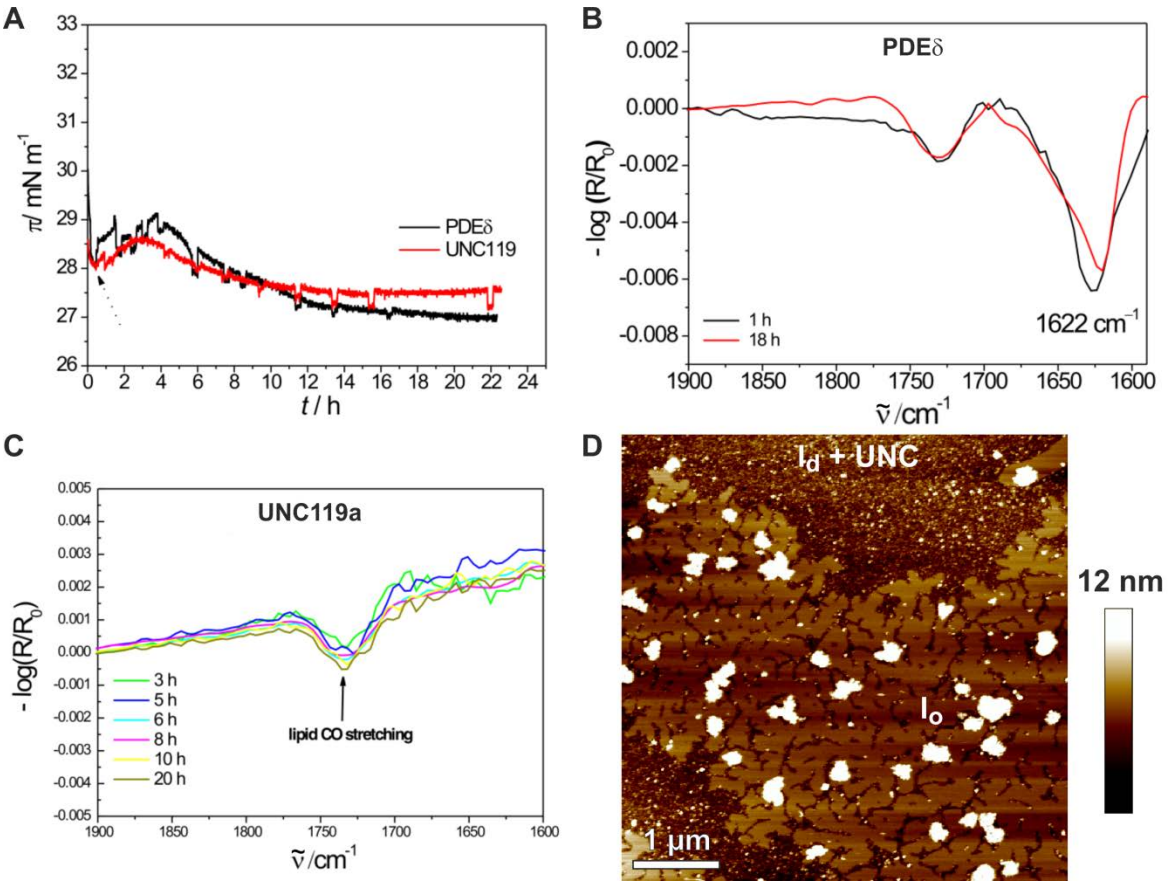

FIGURE S4 Membrane interaction of UNC119a in comparison to PDEδ. (A) Surface pressure/time isotherms for the interaction of PDEδ and UNC119a with anionic lipid raft membranes. Corresponding IRRA spectra for the amide-I′ region of PDEδ (B) and UNC119a (C) in the presence of anionic monolayers. All IRRA spectra were recorded with p-polarized light at 35° angle of incidence. (D) AFM image of the membrane interaction of UNC119a.

Even though membrane interaction of UNC119a seems to be weaker as compared to the other proteins, there is direct evidence in the SPR, IRRAS, and AFM data. Although changes in surface pressure are rather small for UNC119a, the structurally related protein PDEδ (delta subunit of type 6 phosphodiesterase) showed a similar effect on surface pressure upon membrane interaction. Whereas no amide-I′ band could be detected in the IRRA spectra for UNC119a in the presence of anionic model raft membranes, PDEδ exhibited a strong IRRAS amide-I′ band intensity centered at 1622 cm^{-1}, being indicative for the β-sheets of the immunoglobulin-like β-sandwich structure. This point toward a strong adsorption of PDEδ at, but no insertion into, the lipid monolayer. The absence of an amide-I′ band for UNC119a suggests a weak membrane interaction profile. In addition, SPR sensorgrams revealed some binding of UNC119a to anionic model membranes, even though the initial slope is low (cf. Fig. 6A, B). Finally, complementary AFM measurements show a binding of UNC119a to l_d domains of phase-separated membranes, with small protein clusters being detectable. The larger amount of proteins detected in the AFM images as compared to IRRAS can be explained by the different instrumental setups: In IRRAS the proteins are injected in the subphase of the Langmuir trough underneath the lipid monolayer and thus need to diffuse (upwards) to the lipid/air interface. In contrast, in the AFM fluid cell the protein solution is injected across the mica-supported lipid bilayer.

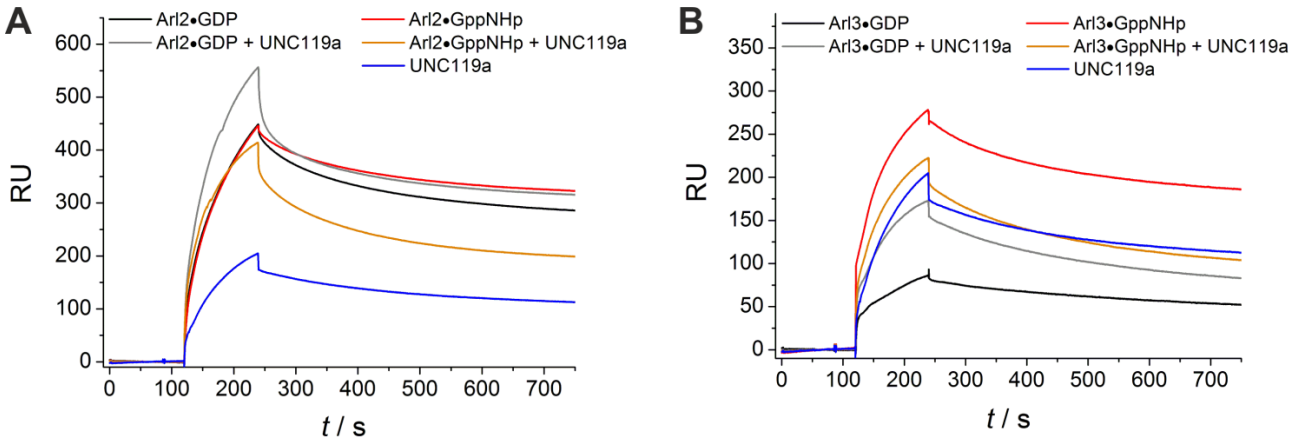

FIGURE S5 Effect of UNC119a on the SPR sensorgrams of Arl2 (A) and Arl3 (B) in the presence of anionic raft membranes.

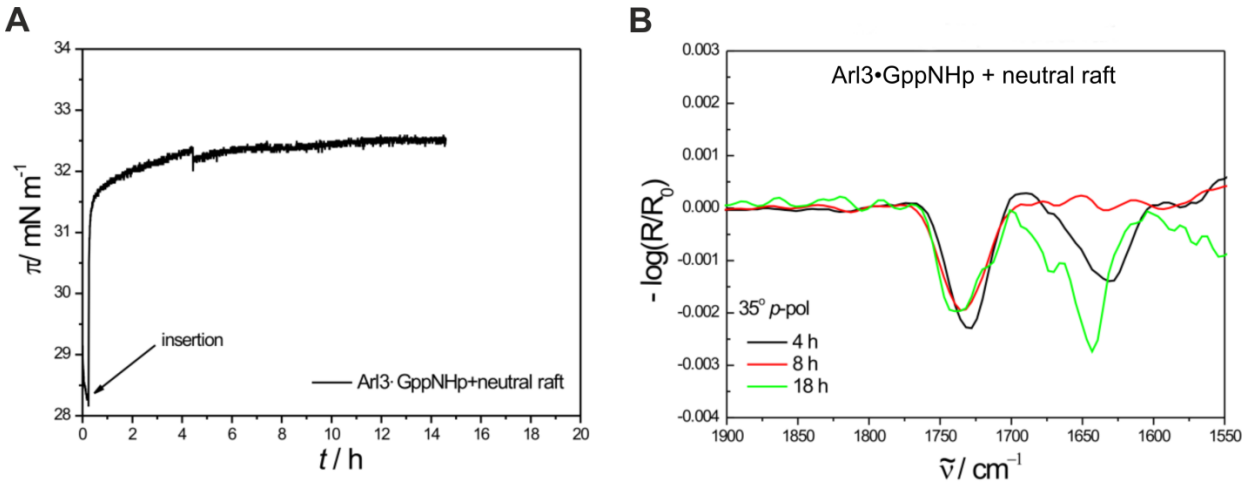

FIGURE S6 Interaction of GppNHp-loaded Arl3 with zwitterionic lipid raft monolayers composed of DOPC/DPPC/Chol 25:50:25 (mol %). (A) Surface pressure/time isotherm for the membrane binding of Arl3•GppNHp to neutral lipid raft monolayers. (B) Corresponding time-dependent IRRA spectra for the amide-I′ region of membrane-bound Arl3•GppNHp. All IRRA spectra were recorded with p-polarized light at 35° angle of incidence. Whereas the surface pressure profile reveals no significant differences to the binding of Arl3•GppNHp to anionic lipid raft monolayers ($\Delta\pi \approx$ 3-4 mN/m, cf. Fig. 2C), the intensity of the amide-I′ band in the concomitant IRRA spectra is about two-fold less upon binding of Arl3•GppNHp to neutral lipid raft membranes (cf. Fig. 2D), which can be due to a different orientation of the protein at the membrane. The results demonstrate that membrane insertion of the N-terminal helix of Arl3•GppNHp occurs independently of the membrane composition and presence of negatively charged lipids.

TABLES

Table S1: Summary of all kinetic parameters of the interaction of GDP- and GppNHp-loaded Arl2 as well as truncated, GppNHp-loaded Arl2 with membranes composed of DOPC/DOPG/DPPC/DPPG/Chol 20:5:45:5:25 (mol %). In the table, the mean value ± standard deviation (n = 3-5) is given.

	Arl2•GDP	Arl2•GppNHp	ΔArl2•GppNHp
$k_{on,1}$ / M^{-1} s^{-1}	$1.50\times10^4 \pm 6.89\times10^3$	$1.03\times10^4 \pm 1.84\times10^3$	$2.07\times10^4 \pm 2.93\times10^4$
$k_{on,2}$ / s^{-1}	$0.003 \pm 8.47\times10^{-4}$	$0.003 \pm 1.68\times10^{-4}$	$0.002 \pm 8.80\times10^{-4}$
$k_{off,1}$ / s^{-1}	0.012 ± 0.012	0.011 ± 0.008	0.015 ± 0.002
$k_{off,2}$ / s^{-1}	0.013 ± 0.010	0.015 ± 0.014	$0.003 \pm 3.44\times10^{-4}$
$\bar{k}_{diss}$ / s^{-1}	0.009 ± 0.001	0.008 ± 0.001	0.006 ± 0.002
quasi-irrev. bound protein / %	62.77 ± 5.08	69.06 ± 2.25	64.84 ± 2.98
initial slope / RU s^{-1}	17.08 ± 2.01	12.33 ± 1.36	3.25 ± 1.63

Table S2: Summary of all kinetic parameters of the interaction of GDP- and GppNHp-loaded Arl3 as well as truncated, GppNHp-loaded Arl3 with membranes composed of DOPC/DOPG/DPPC/DPPG/Chol 20:5:45:5:25 (mol %). In the table, the mean value ± standard deviation (n = 3-6) is given.

	Arl3•GDP	Arl3•GppNHp	ΔArl3•GppNHp
$k_{on,1}$ / M^{-1} s^{-1}	$1.30\times10^4 \pm 2.30\times10^3$	$2.53\times10^4 \pm 2.16\times10^4$	$2.07\times10^4 \pm 8.64\times10^3$
$k_{on,2}$ / s^{-1}	$0.001 \pm 7.22\times10^{-4}$	$0.002 \pm 4.15\times10^{-4}$	0.003 ± 0.002
$k_{off,1}$ / s^{-1}	0.009 ± 0.009	0.011 ± 0.006	0.013 ± 0.007
$k_{off,2}$ / s^{-1}	$0.001 \pm 4.68\times10^{-4}$	0.006 ± 0.007	0.006 ± 0.005
$\bar{k}_{diss}$ / s^{-1}	0.002 ± 0.001	$0.006 \pm 9.00\times10^{-4}$	$0.006 \pm 5.73\times10^{-4}$
quasi-irrev. bound protein / %	44.44 ± 9.45	60.07 ± 3.30	54.31 ± 4.49
initial slope / RU s^{-1}	14.93 ± 1.71	79.33 ± 6.20	7.41 ± 1.19

Table S3: Summary of all kinetic parameters of the interaction of UNC119a-complexed, GDP- and GppNHp-loaded Arl2 and Arl3 as well as UNC119a alone with membranes composed of DOPC/DOPG/DPPC/DPPG/Chol 20:5:45:5:25 (mol %). In the table, the mean value ± standard deviation (n = 3-4) is given.

	Arl2•GDP + UNC119a	Arl2•GppNHp + UNC119a	Arl3•GDP + UNC119a	Arl3•GppNHp + UNC119a	UNC119a
$k_{on,1}$ / M^{-1} s^{-1}	$1.09\times10^{4} \pm 2.29\times10^{3}$	$1.25\times10^{4} \pm 1.48\times10^{3}$	$1.32\times10^{4} \pm 1.88\times10^{3}$	$1.37\times10^{4} \pm 2.56\times10^{3}$	$8.14\times10^{3} \pm 2.28\times10^{3}$
$k_{on,2}$ / s^{-1}	$0.004 \pm 1.45\times10^{-4}$	0.004 ± 0.001	$0.002 \pm 3.76\times10^{-4}$	0.013 ± 0.009	$0.002 \pm 6.66\times10^{-4}$
$k_{off,1}$ / s^{-1}	0.085 ± 0.015	0.056 ± 0.025	0.005 ± 0.004	0.004 ± 0.004	0.005 ± 0.005
$k_{off,2}$ / s^{-1}	$0.005 \pm 3.22\times10^{-4}$	$0.005 \pm 5.77\times10^{-5}$	0.006 ± 0.004	0.010 ± 0.005	0.010 ± 0.009
$\bar{k}_{diss}$ / s^{-1}	0.034 ± 0.003	0.027 ± 0.017	$0.004 \pm 4.64\times10^{-4}$	$0.005 \pm 3.69\times10^{-4}$	0.005 ± 0.002
quasi-irrev. bound protein / %	62.78 ± 2.52	55.16 ± 3.48	43.03 ± 5.86	43.29 ± 5.04	60.17 ± 3.68
initial slope / RU s^{-1}	31.26 ± 1.25	22.30 ± 1.08	18.64 ± 1.33	18.93 ± 1.63	7.19 ± 0.15

SUPPORTING REFERENCES

1. Gohlke, A., G. Triola, H. Waldmann, and R. Winter. 2010. Influence of the lipid anchor motif of N-ras on the interaction with lipid membranes: a surface plasmon resonance study. *Biophys. J.* 98:2226–2235.
2. Cooper, M. A., A. Hansson, S. Löfås, and D. H. Williams. 2000. A vesicle capture sensor chip for kinetic analysis of interactions with membrane-bound receptors. *Anal. Biochem.* 277:196–205.
3. Besenicar, M., P. Macek, J. H. Lakey, and G. Anderluh. 2006. Surface plasmon resonance in protein-membrane interactions. *Chem. Phys. Lipids.* 141:169–178.
4. Mozsolits, H., W. G. Thomas, and M. I. Aguilar. 2003. Surface plasmon resonance spectroscopy in the study of membrane-mediated cell signalling. *J. Pept. Sci.* 9:77–89.
5. Weise, K., S. Kapoor, C. Denter, J. Nikolaus, N. Opitz, S. Koch, G. Triola, A. Herrmann, H. Waldmann, and R. Winter. 2011. Membrane-mediated induction and sorting of K-Ras microdomain signaling platforms. *J. Am. Chem. Soc.* 133:880–887.
6. Mendelsohn, R., G. Mao, and C. R. Flach. 2010. Infrared reflection-absorption spectroscopy: principles and applications to lipid-protein interaction in Langmuir films. *Biochim. Biophys. Acta.* 1798:788–800.